Investigation of microstructure and liquid lead corrosion behavior of a Fe-18Ni-16Cr-4Al base alumina-forming austenitic stainless steel

Materials Research Express

PAPER

Investigation of microstructure and liquid lead corrosion behavior of a Fe-18Ni-16Cr-4Al base alumina-forming austenitic stainless steel

Lingzhi Chen[1], **Man Wang**[2], **Valentyn Tsisar**[3], **Carsten Schroer**[3] **and Zhangjian Zhou**[1]

[1] School of Materials Science and Engineering, University of Science and Technology Beijing, Beijing 100083, People's Republic of China
[2] College of Material Science and Engineering, Beijing University of Technology, Beijing 100124, People's Republic of China
[3] Karlsruhe Institute of Technology (KIT), Institute for Applied Materials-Applied Materials Physics, Karlsruhe 76344, Germany

E-mail: zhouzhj@mater.ustb.edu.cn

Keywords: microstructure, liquid lead, corrosion behavior, Alumina-forming austenitic steel

OPEN ACCESS

RECEIVED
31 October 2019

REVISED
28 January 2020

ACCEPTED FOR PUBLICATION
30 January 2020

PUBLISHED
10 February 2020

Abstract

The microstructure of an alumina-forming austenitic stainless steel with a composition design of Fe-18Ni-16Cr-4Al-2Mo-0.4 Nb (in wt%) is characterized. The steel contains about 75 vol% austenitic phase and 25 vol% ferritic phase. B2-NiAl precipitates with round shape can be found only in the ferritic phase in the as-rolled sample. The corrosion behavior in static liquid lead with different oxygen content of 10^{-9} and 10^{-6}% by mass at 700 °C for 1000 h is investigated. After exposure for 1000 h in liquid lead with oxygen content of 10^{-9}%, obvious lead penetration combined with nickel dissolution is found. In the case of liquid lead with 10^{-6}% oxygen content, a thin oxide layer can be formed on the surface, thus protecting the steel from liquid lead attack. After the corrosion test, significant precipitations are found in both austenitic and ferritic phases in the matrix of the steel.

1. Introduction

In the near future, a number of advanced energy systems will operate at a rather high temperature level in order to improve the thermal efficiency and decrease the CO_2 emission. For example, the service temperature of ultra-supercritical power plant will increase from the current level of 600 °C to 700 °C [1], some advanced nuclear energy systems will also operate at temperature between 600 to 700 °C [2]. It is important to develop new grade high temperature steels for the core component application in these energy systems, as the strength of current applied steels cannot meet the service requirement if the operation temperature is higher than 600 to 650 °C [3–5]. Especially, these advanced energy systems will use corrosive fluid, such as supercritical water, or liquid metal as coolant and thermal exchange medium. Among them, liquid metal, such as liquid lead shows more serious corrosion problems to the contact materials, as significant dissolution of the main elements in steels, such as Ni, Cr, Fe, will occur in high temperature liquid lead [6–8].

Recently, a new type of aluminum alloyed austenitic steel, named as alumina-forming austenitic (AFA) steel, has been developed based on the high temperature ultrafine precipitate strengthening steel in Oak Ridge National Laboratory [9–11]. It is demonstrated that the addition of Al in austenitic steels can not only increase the high temperature strength, but also improve the corrosion resistance significantly [11, 12]. The AFA steels show good creep performance in the temperature range of 600 °C–900 °C due to the precipitation strengthening of NbC, NiAl, and Laves phases, which have better high temperature stability than $M_{23}C_6$ phase, the most important strengthen phase in the traditional steels [13]. The good oxidation/corrosion resistance of AFA steels is thanks to the surface formed dense thin Al_2O_3 scales, which is much more thermodynamic stable compared with the traditional Cr_2O_3 protective scale at high temperature in many aggressive environments [14–16]. A number of research works have demonstrated the excellent corrosion resistance of AFA steels in high temperature dry air, steam and super critical water. Preliminary works also show promising corrosion resistance of AFA steels in oxygen controlled liquid lead based alloy [17].

The diffusion ability of Al in the matrix of steels is a key factor to form a thin protective scale during exposure in corrosive medium. Al_2O_3 scale is usually used in FeCrAl ferritic steels, as Al is a strong ferrite forming element

and its diffusion rate in ferrite is higher than that in austenite. Dense continuous Al_2O_3 scale is not easy to form on the surface of austenitic steels, especially if temperature is higher than the internal oxidation transition temperature, as internal oxidation of Al will easy occur, thus destroy the formation of protective Al_2O_3 scale. Austenitic-ferritic duplex stainless steel can provide an attractive combination of mechanical properties and corrosion resistance, which is considered a promising material for advanced reactors [18, 19]. It can suppose that introduction ferritic phase into the AFA steel will be benefit for the formation of protective Al_2O_3 scale due to the better diffusion ability of Al in ferritic phase than in austenitic phase, thus improve its corrosion resistance.

In this work, an alumina forming austenitic steel containing ferritic phase is fabricated. Its corrosion behavior in statistic liquid lead with different oxygen concentrations at 700 °C has been investigated preliminarily. The effect of oxygen contents on the liquid lead corrosion resistance is discussed. The microstructures, especially precipitation, before and after corrosion test have been characterized and compared.

2. Experimental

2.1. Materials and microstructure characterization

The investigated steel was fabricated by vacuum induction melting and hot deformation. The casting ingot was forged to a plate at 1230 °C with a forging ratio of 3:1, then it was hot rolled at 1200 °C with a total thickness reduction of 80%.

The designed nominal composition of the steel is Fe-18Ni-16Cr-4Al-2Mo-0.4 Nb (in wt%). The actual chemical composition was measured by inductively coupled plasma optical emission spectrometry (ICP-OES), which is Fe-17.91Ni-16.25Cr-1.82Mo-3.29Al-0.35 Nb (in wt%). Phases was characterized by x-ray diffractometer (XRD, RIGAKU d/MAX-2500).

Scanning electron microscope (SEM, JSM-7100F) equipped with an energy dispersive spectrometer (EDS) was used for microstructure and composition characterization of samples before and after corrosion test. Electron backscatter diffraction (EBSD) in conjunction with a field-emission scanning electron microscopy (FE-SEM, ZEISS ULTRA55) was used for the characterization of grain and phase distribution.

To characterize the precipitates, a transmission electron microscope (TEM, JEM-2010) with a resolution of 0.2 nm was operated at an accelerating voltage of 200 kV. The TEM foil sample was prepared by two in-jet polishing using 10 vol% $HClO_4$ + 90 vol% C_2H_5OH.

2.2. Corrosion test

The samples for corrosion test are in cylindrical shape with a nominal dimension of Ø8 mm × 15 mm cutting from the rolled steel plate. The surface of the samples were machined by fine-turning, cleaned and degreased in acetone. The samples were fitted into alumina crucibles using Mo holders, then immersed into stagnant liquid lead. One purpose of this work is to investigate the effect of oxygen content in liquid lead on the corrosion behavior of the AFA steel, thus two tests were performed in liquid lead with different dissolved oxygen concentrations at 700 °C, and the exposure time are all set at 1000 h. The oxygen concentration in the liquid lead was controlled using a flowing gas mixture containing Ar, H_2 and air introduced above the liquid surface. Two Pt/air oxygen sensors monitored the success of oxygen control during the whole testing period. The dissolved oxygen concentration was calculated from the sensor output.

After the corrosion test, all samples were cut in half along the radial direction for the cross section microstructure analysis. The metallographic specimen was prepared by cold mounting resin to avoid re-melting of the adherent lead which was usually maintained to protect the corrosion layer before the cross section analysis.

3. Results and discussion

3.1. Microstructure characterization

Figure 1(a) shows the SEM morphology of the as rolled sample. It is obvious that the material consists two phases. According to EDS analysis, the phase with light contrast contains more Cr and Al, but less Ni, compared with the dark contrast phase. Further EBSD analysis confirm that the phase with light contrast is ferrite accounting for 25% in volume fraction, while the other 75% is austenite, as seen in figure1(c). The grains in both phases are obviously deformed along the hot rolling direction. The austenitic phase is quite clean, while the ferritic phase seems to contain a lot of precipitates, as indicated by arrows in figure 1(b).

TEM analysis was performed to characterize the precipitates distributed in the ferritic phase. The TEM morphology in figure 2(a) shows that the precipitates have a round shape, the particle size is between 50 nm to 100 nm based on measurement of 3 different pictures. These precipitates are rich Ni and Al according to the EDS analysis. Further selected area electron diffraction (SAED) demonstrates they are B2-NiAl intermetallic phase

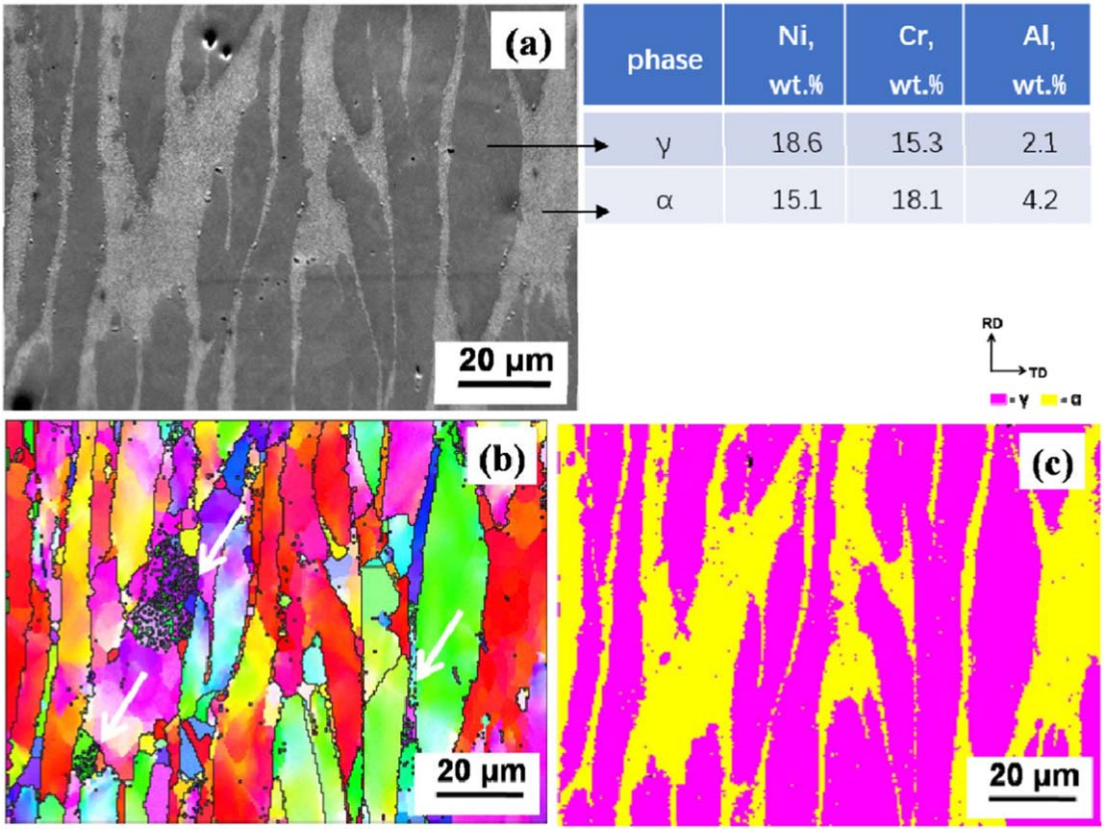

Figure 1. The microstructure of the steel, (a) SEM morphology, (b) EBSD shows the orientation of the grains, and (c) phase distribution.

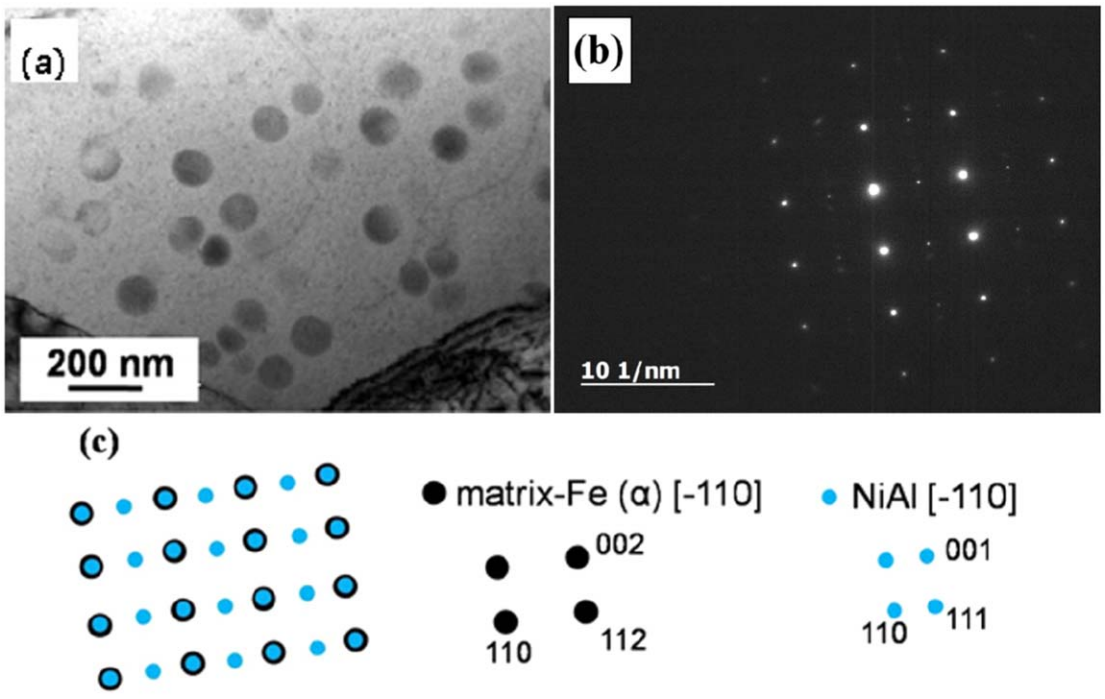

Figure 2. TEM analysis of the precipitates formed in the ferritic phase, (a) morphology of the precipitates, (b) SAED, (c) sketch map of the calibration of the diffraction patterns.

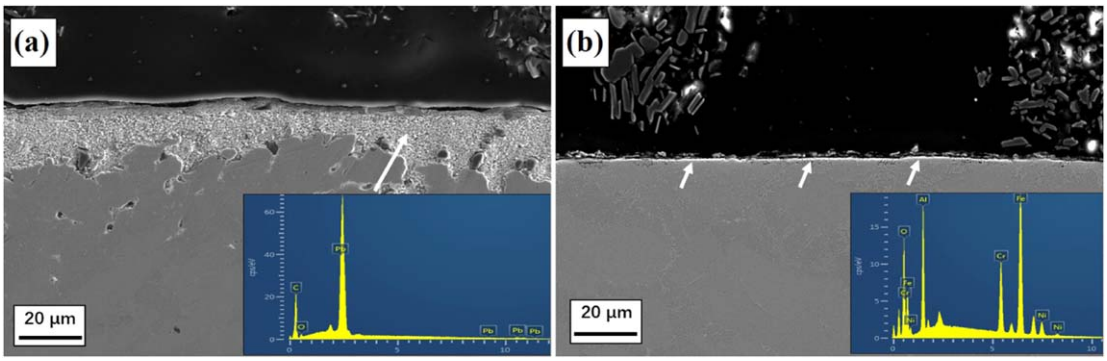

Figure 3. Cross section SEM morphology of AFA steel after exposure in the liquid lead with oxygen content of 10^{-9} mass % (a), and 10^{-6} mass % (b).

(PDF#44-1188, Pm3m), as seen in figures 2(b) and (c). There is a certain orientation relationship, namely $(002)_M//(001)_P$ and $[-110]_M//[-110]_P$, between the ferrite matrix and precipitates. It should be noted that these round B2-NiAl precipitates are only observed in the ferritic phase in the as-rolled sample. The reason is that the lattice misfit between NiAl and ferrite is very small, only 0.4%, while it is nearly 20% between NiAl and austenite, thus NiAl phase is much easier to precipitate in the ferritic phase than in the austenitic phase during the fabrication process [20].

3.2. Corrosion behavior in liquid lead

Figure 3 shows the typical cross section SEM morphology and EDS analysis of the AFA samples after exposure for 1000 h in the liquid lead with different oxygen content at 700 °C. Significant corrosion occurs in the case of 10^{-9} mass % oxygen concentration, as seen in figure 3(a). Lead with light contrast adhered on the surface and penetrated deep into the matrix. This result is similar to the corrosion behavior of the traditional austenitic steels in liquid lead based alloy [6–8]. The penetration of Pb is due to the selective dissolution of Ni in liquid lead at such low oxygen concentration. When the oxygen concentration achieves 10^{-6} mass % in the liquid lead, a very thin scale is found on the surface of the sample, as indicated by the arrows in figure 3(b). Almost no dissolution type corrosion and lead penetration can be detected. EDS analysis demonstrated that the scale is Al and Cr rich oxide layer. The thickness of the scale is less than 1 μm. This result demonstrates that for the Al alloyed steel in this work, oxygen content should be controlled to the level of 10^{-6} mass % in the liquid lead at 700 °C to promote the formation of a stable thin protective oxide scale.

3.3. Microstructure evolution after corrosion test

In our previous work, obvious precipitation was found in the AFA steel after annealing at 950 °C only for 50 h [20]. As the corrosion test was performed at 700 °C for a long time, it can suppose that similar precipitation may occur during the corrosion test. Figure 4 shows the SEM morphology of the matrix and EDS analysis of the precipitates far away from the surface oxidation scale after exposure in the liquid lead with oxygen concentration of 10^{-6} mass %. A large amount of precipitates are found not only in the ferritic phase but also in the austenitic phase. SEM morphology with high magnification shows that there are three kinds of precipitates: round particles with dark contrast in the ferric phase, needle shape particles with dark contrast in the austenitic phase, and columnar precipitates with light contrast formed in the ferritic phase as well as in the austenitic phase. Both round particles and needle particles with dark contrast are rich Ni and Al, and the white columnar particles rich Fe and Nb according to EDS analysis. These results are similar to our previous work, which demonstrate that the round and needle shape precipitates are B2-NiAl, and the white columnar precipitate is Laves Fe_2Nb [20].

It should be noted that the size of some round NiAl particles in the ferritic phase are quite large, around 200 to 500 nm, as seen in figure 4(c), which indicates the coarsen of the initial NiAl particles in the as-rolled material after long time exposure in liquid lead at 700 °C. There are also some small round NiAl particles which are always adjoint with the columnar Laves phase. Similar phenomena is found in the austenitic phase as well, the needle NiAl particles are connected with columnar Laves particles. If compared with the as-rolled sample, it can be supposed that all these precipitates should be formed during the long time corrosion test. This result is agree with the reported works that the formation of Laves phase can accelerate the precipitate of NiAl phase, thus they are always connected each other [21, 22].

Figure 5 shows the XRD diffraction patterns of the original sample and sample after corrosion test in 700 °C liquid lead with 10^{-6} mass % oxygen content for 1000 h. Both samples contain austenitic phase and ferritic

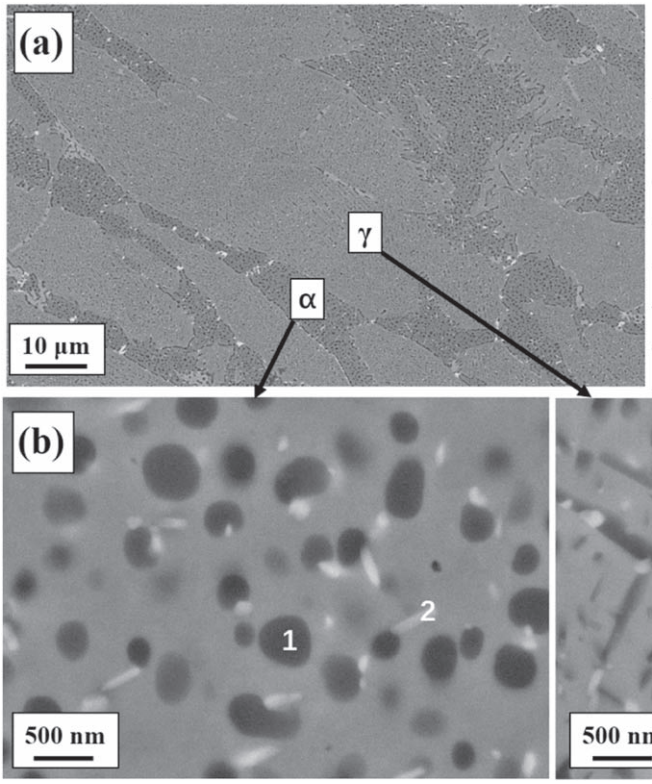

EDS result of precipitates indicated in image (b) and (c), in at. %

element	1	2	3	4
Fe	36.5	50.4	30.4	50.1
Cr	9.1	14.8	12.6	13.4
Ni	33.7	5.5	32.8	6.2
Al	20.7	3.3	22.7	2.9
Mo	-	19.8	1.5	21.3
Nb	-	6.2	-	6.1

Figure 4. The microstructure evolution after exposure in liquid lead for 1000 h at 700 °C, (a) duplex morphology, (b) round shape NiAl and column Fe_2Nb precipitates formed in the ferritic phase, (c) needle shape NiAl and column Fe_2Nb precipitates in the austenitic phase.

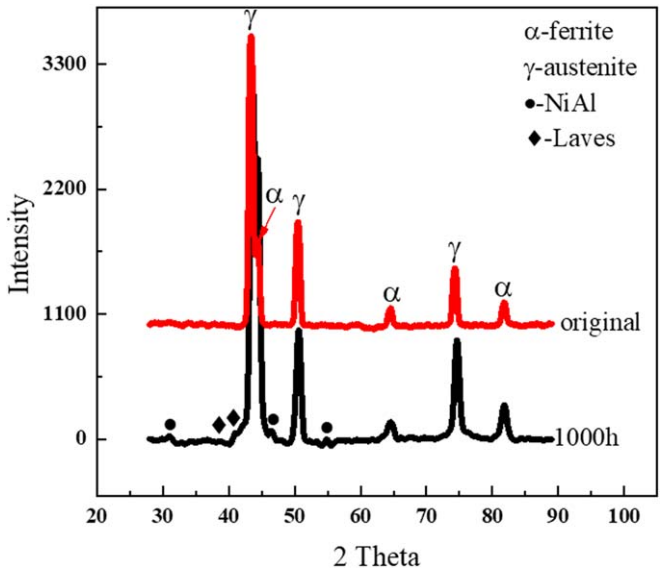

Figure 5. XRD patterns of samples before corrosion test and after corrosion test for 1000 h.

phase. NiAl and Laves phase can be observed in the 1000 h tested sample, this result is agree with the SEM observation.

Although Laves phase usually is considered detrimental for mechanical property of traditional steels [23]. Some research works also demonstrate the strengthen effect of Laves phase in austenitic steels, as the lattice misfit degree between Laves phase and austenitic phase is very small, and the precipitate with low misfit to matrix can improve mechanical property [24–27]. Apart from potential strengthen effect, Laves phase is also benefit for the precipitation of B2-NiAl phase, which is considered not only an important strengthen phase for Fe-Ni-Cr-Al

alloy [9, 12], but also important to the oxidation resistance of the steels. As NiAl can continuous supply Al for the formation of dense continuous alumina scale, namely provide a reservoir effect [15, 28–31]. For better understanding the performance of alumina forming austenitic stainless steels, it is necessary to pay more attention on the annealing behavior of the precipitates and investigate their strengthen effects.

4. Conclusions

The microstructure and preliminary corrosion behavior of an alumina forming austenitic stainless steel in liquid lead at 700 °C with different oxygen concentration were investigated. The conclusions are as follows:

(1) The AFA steel with composition of Fe-17.91Ni-16.25Cr-1.82Mo-3.29Al-0.35 Nb contains 75% austenite and 25% ferrite. Round shape B2 NiAl precipitates only formed in ferrite in the as-rolled sample.

(2) Obvious dissolution based corrosion and penetration of lead occur after exposure in 700 °C liquid lead with very low oxygen concentration. The material shows very good corrosion resistance in 700 °C liquid lead when the oxygen concentration is controlled at the level of 10^{-6} mass %.

(3) After long term exposure in liquid lead at 700 °C, obvious coarsen can be found for the initial round NiAl particles in ferrite. Small round NiAl particles and needle NiAl particles will form in ferrite and austenite respectively, columnar Laves phase will form in both ferrite and austenite.

Acknowledgments

The authors would like to thank for the financial support by the International Science and Technology Cooperation Program of China (No. 2018YFE0116200). The corrosion tests in liquid lead were financially supported by the Renewable Energies (RE) Program of KIT.

ORCID iDs

Zhangjian Zhou https://orcid.org/0000-0002-2240-0772

References

[1] Fujio A 2015 *Research and Development of Heat-Resistant Materials for Advanced USC Power Plants with Steam Temperatures of 700 °C and Above, Engineering* **1** 211–24
[2] Buckthorpe D 2017 *Introduction to Generation IV nuclear reactors, in Structural Materials for Generation IV Nuclear Reactors [M]* (Amsterdam: Elsevier)
[3] Zinkle S J, Boutard J L, Hoelzer D T, Kimura A, Lindau R, Odette G R, Rieth M, Tan L and Tanigawa H 2017 Development of next generation tempered and ODS reduced activation ferritic/martensitic steels for fusion energy applications *Nucl. Fusion* **57** 092005
[4] Murty K L and Charit I 2008 Structural materials for gen-IV nuclear reactors: challenges and opportunities *J. Nucl. Mater.* **383** 189–95
[5] Hosemann P, Frazer D, Fratoni M, Bolind A and Ashby M F 2018 Materials selection for nuclear applications: challenges and opportunities *Scr. Mater.* **143** 181–7
[6] Yamaki E, Ginestar K and Martinelli L 2011 Dissolution mechanism of 316L in lead–bismuth eutectic at 500 °C *Corros. Sci.* **53** 3075–85
[7] Schroer C, Wedemeyer O, Novotny J, Skrypnik A and Konys J 2014 Selective leaching of nickel and chromium from Type 316 austenitic steel in oxygen-containing lead-bismuth eutectic (LBE) *Corros. Sci.* **84** 113–24
[8] Caro M, Woloshun K, Rubio F, Maloy S A and Hosemann P 2013 Heavy liquid metal corrosion of structural materials in advanced nuclear systems *JOM* **65** 1057–66
[9] Yamamoto Y, Brady M P, Lu Z P, Maziasz P J, Liu C T, Pint B A, More K L, Meyer H M and Payzant E A 2007 Creep-resistant, Al2O3-forming austenitic stainless steels *Science* **316** 433–6
[10] Yamamoto Y, Santella M L, Liu C T, Evans N D, Maziasz P J and Brady M P 2009 Evaluation of Mn substitution for Ni in alumina-forming austenitic stainless steels *Mater. Sci. Eng., A* **524** 176–85
[11] Brady M P, Magee J, Yamamoto Y, Helmick D and Wang L 2014 Co-optimization of wrought alumina-forming austenitic stainless steel composition ranges for high-temperature creep and oxidation/corrosion resistance *Mater. Sci. Eng., A* **590** 101–15
[12] Yamamoto Y, Takeyama M, Lu Z P, Liu C T, Evans N D, Maziasz P J and Brady M P 2008 Alloying effects on creep and oxidation resistance of austenitic stainless steel alloys employing intermetallic precipitates *Intermetallics* **16** 453–62
[13] Yamamoto Y, Brady M P, Lu Z P, Liu C T, Takeyama M, Maziasz P J and Pint B A 2007 Alumina-forming austenitic stainless steels strengthened by laves phase and MC carbide precipitates *Metallurgical and Materials Transactions A* **38A** 2737–46
[14] Brady M P, Yamamoto Y, Santella M L and Pint B A 2007 Effects of minor alloy additions and oxidation temperature on protective alumina scale formation in creep-resistant austenitic stainless steels *Scr. Mater.* **57** 1117–20
[15] Brady M P, Gleeson B and Wright I G 2000 Alloy design strategies for promoting protective oxide-scale formation *JOM* **52** 16–21
[16] Sun S, Zhou Z, Zhang L and Tang R 2018 Oxidation behavior and stress corrosion cracking susceptibility of Fe27Ni16Cr3.5Al based AFA alloy in supercritical water *Mater. Res. Express* **5** 066525
[17] Ejenstam J and Szakálos P 2015 Long term corrosion resistance of alumina forming austenitic stainless steels in liquid lead *J. Nucl. Mater.* **461** 164–70

[18] Malta P O, Dias F L, de Souza A C M and Santos D B 2018 Microstructure and texture evolution of duplex stainless steels with different molybdenum contents *Mater. Charact.* **142** 406–21
[19] Kim H, Jang H, Subramanian G O, Kim C W and Jang C H 2018 Development of alumina-forming duplex stainless steels as accident tolerant fuel cladding materials for light water reactors *J. Nucl. Mater.* **507** 1–14
[20] Wang M, Sun Y, Feng J, Zhang R, Tang R and Zhou Z 2016 Microstructural evolution and mechanical properties of an Fe-18Ni-16Cr-4Al base alloy during aging at 950 °C *Int. J. Miner. Metall. Mater.* **23** 314–22
[21] Zhou D *et al* 2015 Precipitate characteristics and their effects on the high-temperature creep resistance of alumina-forming austenitic stainless steels *Mater. Sci. Eng., A* **622** 91–100
[22] Trotter G and Baker I 2015 Orientation relationships of Laves phase and NiAl particles in an AFA stainless steel *Philos. Mag.* **95** 4078–94
[23] Chen S, Zhang C, Xia Z, Ishikawa H and Yang Z 2014 Precipitation behavior of Fe_2Nb Laves phase on grain boundaries in austenitic heat resistant steels *Mater. Sci. Eng., A* **616** 183–8
[24] Wen D H, Li Z, Jiang B B, Wang Q, Chen G Q, Tang R, Zhang R Q, Dong C and Liaw P K 2018 Effects of Nb/Ti/V/Ta on phase precipitation and oxidation resistance at 1073 K in alumina-forming austenitic stainless steels *Mater. Charact.* **144** 86–98
[25] Sauthoff G 2000 Multiphase intermetallic alloys for structural applications *Intermetallics* **8** 1101–9
[26] Yamamoto K, Kimura Y, Wei F G and Mishima Y 2002 Design of Laves phase strengthened ferritic heat resisting steels in the Fe-Cr-Nb (-Ni) system *Mater. Sci. Eng., A* **329** 249–54
[27] Wang M, Sun H, Phaniraj M P, Han H N, Jang J and Zhou Z 2016 Evolution of microstructure and tensile properties of Fe–18Ni–12Cr based AFA steel during aging at 700 °C *Materials Science & Engineering A* **672** 23–31
[28] Brady M, Unocic K A, Lance M J, Santella M, Yamamoto Y and Walker L 2011 Increasing the upper temperature oxidation limit of alumina forming austenitic stainless steels in air with water vapor *Oxidation of Metal* **75** 337–57
[29] Saunders S, Monteiro M and Rizzo F 2008 The oxidation behavior of metals and alloys at high temperatures in atmospheres containing water vapor: a review *Progress of Materials Science* **53** 775–837
[30] Xu X Q, Zhang X F, Chen G L and Lu Z P 2011 Improvement of high-temperature oxidation resistance and strength in alumina-forming austenitic stainless steels *Materials Letter* **65** 3285–8
[31] Brady M, Yamamoto Y, Santella M and Walker L 2009 Composition, microstructure, and water vapor effects on internal/external oxidation of alumina-forming austenitic stainless steels *Oxidation of Metal* **72** 311–33